Dyes and Pigments 100 (2014) 278–285

Contents lists available at ScienceDirect

Dyes and Pigments

journal homepage: www.elsevier.com/locate/dyepig

A key point of porphyrin structure affect DSSCs performance based on porphyrin sensitizers

Zhe Zeng [a], Bao Zhang [a], Chengjie Li [a], Xiao Peng [a], Xiujun Liu [a], Shuxian Meng [a,*], Yaqing Feng [a,b,**]

[a] School of Chemical Engineering and Technology, Tianjin University, No.92, Weijin Road, Nankaiwei District, Tianjin 300072, PR China
[b] Tianjin Co-Innovation Center of Chemical Science and Engineering, Tianjin University, Tianjin 300072, PR China

ARTICLE INFO

Article history:
Received 3 May 2013
Received in revised form
29 July 2013
Accepted 29 July 2013
Available online 22 August 2013

Keywords:
Dye-sensitized solar cells
Porphyrin structure
Photovoltaic
β Position
Linker
Sonogashira coupling

ABSTRACT

Two sets of *meso*-tetraphenylzincporphyrins have been synthesized via Sonogashira coupling and Knoevenagel condensation. The photophysical and electrochemical measurements have been performed for each dye, and the photovoltaic properties of all porphyrin-based dye-sensitized solar cells (DSSCs) have been evaluated. For different linkers on β position, meso-substituents show different affections for DSSCs' performances. The matching degree of the length of linker and the size of *meso*-substituent could be a key point in porphyrin structure that affect the cell performance of DSSC based on porphyrin sensitizers. The highest cell performance was achieved with **IId** as a sensitizer and ethanol as an immersing solvent: a short-circuit photocurrent density of 9.75 mA cm^{-2}, an open-circuit voltage of 0.71 V, a fill factor of 0.73, and a light to electricity conversion efficiency of 5.08% under the AM 1.5 sunlight.

1. Introduction

Dye-sensitized solar cells (DSSCs) have attracted significant attention as alternatives to conventional photovoltaic devices based on silicon [1–3]. Although Ruthenium(II) Bipyridyl complexes have been reported to give a solar-to-electrical energy conversion efficiency of up to 11% [1], their extensive application would be hampered considerably owing to the limited resource and the environmental issue [4]. In this regard, a lot of effort has been devoted to develop new and efficient sensitizers suitable for large-scale applications. And many organic dyes such as porphyrins [5–10], coumarins [11–13], perylenes [14], phthalocyanines [15], triarylamines [16], and carbazoles [17] have been paid great attention to because of their modest cost, large molar absorption coefficients and satisfactory stability. Among them, porphyrins due to their strong Soret (400–450 nm) and moderate Q bands (550–600 nm) absorption properties as well as the vital roles of porphyrin derivatives in photosynthesis, have attracted more interests. Moreover, the optical, photophysical, and electrochemical properties of porphyrins can be systematically tailored by the peripheral substitutions and/or inner metal complexations. Therefore, considerable effort has been devoted to investigate the close relationship between molecular structure and photovoltaic properties. For example, Diau et al. [18] introduced π-conjugated PE(phenylethylnyl) unit as a bridging moiety to connect a *meso*-position of ZnBPP and the carboxylic acid end. With different number of PE units, the distance between porphyrin core and TiO_2 surface is different. The efficiency of these porphyrin sensitizers used in DSSC device drop with the length of linker increased systematically. Tian et al. [19] designed a new type metal-free organic dyes, which containing double acceptors without COOH as anchors. Imahori et al. [20] gave the conclusion the cell performance of the porphyrin-sensitized TiO_2 cell was affected greatly by the steric bulkiness around the porphyrin, the electronic coupling between porphyrin core and TiO_2 surface. Since long alkoxyl chain in the *meso*-position of porphyrin can decrease the dye aggregation of efficient electron injection [21], a big *meso*-group could benefit the efficiency of DSSC device. But a large *meso*-group also could affect

* Corresponding author. Tel./fax: +86 022 27892323.
** Corresponding author. School of Chemical Engineering and Technology, Tianjin University, No.92, Weijin Road, Nankaiwei District, Tianjin 300072, PR China.
E-mail addresses: zengzhe_tju@yahoo.cn (Z. Zeng), baozhang@tju.edu.cn (B. Zhang), chengjie_li@tju.edu.cn (C. Li), paladin_x@yahoo.cn (X. Peng), Xiujun_liu@tju.edu.cn (X. Liu), msxmail@tju.edu.cn (S. Meng), yqfeng@tju.edu.cn (Y. Feng).

0143-7208/$ – see front matter © 2013 Elsevier Ltd. All rights reserved.
http://dx.doi.org/10.1016/j.dyepig.2013.07.037

the orientation of porphyrin sensitizers, the surface coverage and performance of DSSC.

In this paper, we report the fundamental properties of various of porphyrins in solution which are adsorbed on TiO_2 nanocrystalline films. Four different substituents (phenyl, *p*-methylphenyl, *p*-isobutylphenyl, *p*-tertbutylphenyl) on *meso*-position and two different linkers (ethylene, phenyl ethynyl) on β position were introduced to porphyrin core. One carboxy group was attached on the linker to ensure the single anchorage of the porphyrin molecular on TiO_2 surface. Preliminary UV–Vis and fluorescence studies were presented in solution. The DSSCs based on these porphyrin sensitizers were fabricated and up to 5.32% conversion efficiency was achieved for porphyrin **IId** under our unoptimized conditions which suggested that porphyrin **IId** is a promising candidate for the cost-effective DSSCs (Fig. 1).

2. Experimental

2.1. Reagents and reagents

All reagents and solvents were obtained from commercial sources and used without further purification, unless otherwise noted. Toluene and THF was dried by distillation from sodium using sodium benzophenone ketyl as indicators prior to use. CH_2Cl_2 was freshly distilled before used for analysis. All chromatographic separations were carried out on silica gel (300–400 mesh or silica H).

2.2. Analytical instruments

^1H NMR spectra were recorded in $CDCl_3$ or DMSO on Varian 500 or Bruker AV400 spectrometer. The chemical shifts were reported in parts per million (δ) relative to the appropriate reference signal: residual chloroform (δ_H 7.26) or DMSO (the quintet centered at 2.50 ppm). MALDI-TOF mass spectra were measured on a Bruker Autoflex Tof/Tof III instrument. IPCE spectra were measured recorded on Quantum efficiency measurement kit. UV–visible spectra of the dyes in CH_2Cl_2 and adsorbed on TiO_2 films at glass plates were recorded with Shimadzu UV-1800 in 10 mm quartz cell spectrometer. The Fluorescence spectra were detected by a Varian Cary Eclipse Spectrometer, emission wavelengths λ were reported in nm. Electrochemical redox potentials were obtained by cyclic voltammetry (CV) using a three-electrode configuration and an electrochemistry workstation (CHI66 660D). The working electrode and the counter electrode were Pt wires. Ag/Ag+ was used as the reference electrode. Tetrabutylammonium perchlorate (TBAP) (0.1 M) was used as the supporting electrolyte in dry CH_2Cl_2. Ferrocene was added to each sample solution at the end of the experiments, and was employed for calibration [22].

2.3. Absorption spectra on TiO_2 films

Absorption spectra of the sensitizers deposited on TiO_2 films were measured with a Shimadzu UV-1800 spectrometer. The TiO_2 films with a typical thickness of 5 μm were dipped into 0.3 mM ethanol solution of chlorin dyes for 15 min and then the dye-adsorbed films are rinsed with ethanol three times and dried in air before measurement of the absorption spectra.

2.4. Measurement of surface coverage (Γ)

TiO_2 films 0.16 cm^2 in size, ~16 μm in thickness were dipped into an ethanolic solution containing each dye sensitizer for 2 h and then washed with ethanol to remove free dye sensitizers on the surface. The adsorbed dye sensitizers were estimated when dissolved in 3 mL of 0.1 M EtONa solution. The absorption spectra of the EtONa solution of each sensitizer were measured to obtain the surface coverage (Γ) according to the standard method [23].

2.5. General procedure for preparation of porphyrin-modified TiO_2 electrode and photovoltaic measurements

The TiO_2 suspension was prepared from P25 following a literature procedure [24]. The film was prepared by screen printing on a precleaned FTO glass. Then the film was annealed to 325 °C for 5 min, 375 °C for 5 min, 450 °C for 15 min, and 500 °C for 15 min. Finally the TiO_2 film was treated with an aqueous $TiCl_4$ solution (50 mM) at 70 °C for 30 min, rinsed with ethanol, and annealed at 500 °C for 30 min. After the film was cooled to 100 °C, the TiO_2 electrode was immersed into the ethanol solutions of dyes (0.3 mM) for 2 h. The sensitized electrode was rinsed with ethanol, and the dried. A sandwich cell consisting of the porphyrin-sensitized TiO_2 electrode being treated as the working electrode and a Pt foil being treated as the counter electrode, was fabricated. The electrolyte (0.06 M LiI, 0.03 M I_2, 0.6 M 1,2-dimethyl-3-propylimidazolium iodide, and 0.5 M 4-tert-butylpyridine in acetonitrile) was injected into the space between two electrodes. The irradiated area of the cell was 0.159 cm^2. The photovoltaic measurements were then performed. The photocurrent–voltage (*J*–*V*) characteristics were recorded on Keithley 2400 Source Meter (solar AAA simulator, oriel China, calibrated with a standard

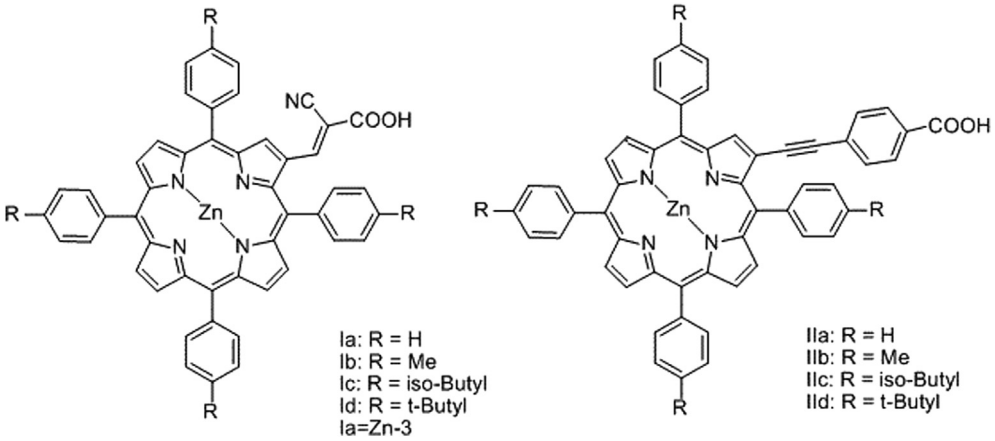

Fig. 1. Molecular structures of porphyrin sensitizers.

crystalline silicon solar). The series of dyes sensitized TiO_2 electrodes were irradiated under simulated AM 1.5 irradiation (100 mW cm^{-2}). The power conversion efficiency (η) of the DSSC was calculated from short-circuit photocurrent (J_{sc}), the open-circuit photovoltage (V_{oc}), the fill factor (FF) and the intensity of the incident light (P_{in}) according to the following equation:

$$\eta = \frac{J_{sc}(\text{mA cm}^{-2}) \times V_{oc}(\text{V}) \times \text{FF}}{P_{in}(\text{mW cm}^{-2})}$$

2.6. Synthesis procedures and characterization data of new compounds

2.6.1. General procedure for the synthesis of *Ia*–*Id*

Compounds **1a**–**1d** were synthesized according to reported method [25]. The synthesis of compounds **Ia**–**Id**: With some modification, Compounds **Ia**–**Id** were synthesized through a similar procedure [26]. Take **Ia** as an example. The solution of **1a** (40 mg), cyanoacetic acid (23.8 mg), zinc acetate (28.8 mg) and ammonium acetate (21.6 mg) in THF (6 mL) was added into acetic acid (6 mL) and heated at reflux temperature for 11 h. The solution was washed with H_2O (300 mL), extracted with chloroform. The solvent was removed in vacuo. The residue was purified by column chromatography using CH_2Cl_2/MeOH (100:1) as eluent, collecting the major green fraction to give **Ia**(**Zn-3**) (29.7 mg, 68%) as a green solid. 1H NMR (400 MHz, DMSO) δ 9.50 (s, 1H,$H_{\beta\text{-pyrroic}}$), 8.86–8.68 (m, 6H,$H_{\beta\text{-pyrroic}}$), 8.25–8.15 (m, 6H,$H_{o\text{-Ph}}$), 8.14–8.06 (m, 3H,2$H_{o\text{-Ph}}$+H–CH=), 7.88–7.74 (m, 12H,$H_{m,p\text{-Ph}}$). MS (MALDI-TOF) *m*/*z* found 771.0 (M^+)(calcd. for $C_{48}H_{29}N_5O_2Zn^+$ 771.1613). UV–vis (CH_2Cl_2) λ_{max} (log ε): 453.6(5.25), 570.8(4.20), 620.2(4.19) nm.

Ib: 15.6 mg, yield 76.4%. ^{1}H NMR (400 MHz, DMSO) δ 9.46 (s, 1H,$H_{\beta\text{-pyrroic}}$), 8.80–8.71 (m, 6H,$H_{\beta\text{-pyrroic}}$), 8.09–8.02 (m, 6H,$H_{o\text{-Ph}}$), 7.98–7.92 (m, 3H,2$H_{o\text{-Ph}}$ + H–CH=), 7.61 (d, J = 7.1 Hz, 6H,$H_{m\text{-Ph}}$), 7.56 (d, J = 7.8 Hz, 2H,$H_{m\text{-Ph}}$), 2.67 (s, 9H,CH_3), 2.63 (s, 3H,CH_3). MS (MALDI-TOF) *m*/*z* found 827.1(M^+)(calcd. for $C_{52}H_{37}N_5O_2Zn^+$ 827.2239). UV–vis (CH_2Cl_2) λ_{max} (log ε): 453.4(5.04), 569.8(4.04), 621.6(4.00) nm.

Ic: 13.3 mg, yield 64.2%. ^{1}H NMR (400 MHz, DMSO) δ 9.52 (s, 1H,$H_{\beta\text{-pyrroic}}$), 8.79 (d, J = 4.7 Hz, 1H,$H_{\beta\text{-pyrroic}}$), 8.76–8.64 (m, 5H,$H_{\beta\text{-pyrroic}}$), 8.12 (s, 1H,H–CH=), 8.07 (d, J = 7.8 Hz, 2H,$H_{o\text{-Ph}}$), 8.05–8.00 (m, 4H,$H_{o\text{-Ph}}$), 7.96 (d, J = 7.7 Hz, 2H,$H_{o\text{-Ph}}$), 7.60–7.46 (m, 8H,$H_{m\text{-Ph}}$), 2.83–2.72 (m, 8H, $-CH_2CH(CH_3)_2$), 2.20–2.07 (m, 4H, $-CH_2CH(CH_3)_2$), 1.10 (s, 24H, $-CH_2CH(CH_3)_2$). MS (MALDI-TOF) *m*/*z* found 995.3(M^+)(calcd. for $C_{64}H_{61}N_5O_2Zn^+$ 995.4117). UV–vis (CH_2Cl_2) λ_{max} (log ε): 454.8(5.13), 571.8(4.10), 623.4(4.08) nm.

Id: 10.2 mg, yield 57.4%. ^{1}H NMR (400 MHz, DMSO) δ 9.42 (s, 1H,$H_{\beta\text{-pyrroic}}$), 8.84 (d, J = 4.6 Hz, 1H,$H_{\beta\text{-pyrroic}}$), 8.78–8.70 (m, 5H,$H_{\beta\text{-pyrroic}}$), 8.16–8.03 (m, 6H,$H_{o\text{-Ph}}$), 8.03–7.95 (m, 3H,2$H_{o\text{-Ph}}$ + H–CH=), 7.86–7.72 (m, 8H,$H_{m\text{-Ph}}$), 1.61–1.52 (m, 36H,CH_3). MS (MALDI-TOF) *m*/*z* found 995.3(M^+)(calcd. for $C_{64}H_{61}N_5O_2Zn^+$ 995.4117). UV–vis (CH_2Cl_2) λ_{max} (log ε): 455.8(4.98), 572.6(4.00), 623.4(3.97) nm.

Table 1
Optical data of all porphyrin sensitizers used in this study.

Dye	λ_{abs}, nm[a] (log ε, $M^{-1}cm^{-1}$)	λ'_{abs}, nm[b]	λ_{em}, nm[c]
Ia	454(5.25),571(4.20),620 (4.19)	625,573,466	652
Ib	453(5.04),570(4.04),622(4.00)	627,573,467	648
Ic	455(5.13),572(4.10),623(4.08)	626,573,467	650
Id	456(4.98),573(4.00),623(3.97)	623,573,463	658
IIa	437(5.13),566(4.00),604 (3.75)	600,565,459	617
IIb	438(5.40),566(4.21),605(3.95)	600,564,456	620
IIc	438(5.43),567(4.26),606(4.00)	597,563,460	620
IId	438(5.53),567(4.34),606(4.07)	603,565,459	622

[a] Absorption data were obtained in CH_2Cl_2 solution.
[b] Absorption data were obtained on TiO_2 film.
[c] Emission spectra were obtained in CH_2Cl_2 by exciting at 434 nm.

2.6.2. General procedure for the synthesis of *IIa*–*IId*

Compounds **2a**–**2d** were synthesized according to reported method [27]. The synthesis of compounds **3a**–**3d**: Compounds **3a**–**3d** were synthesized through a similar procedure as reported with

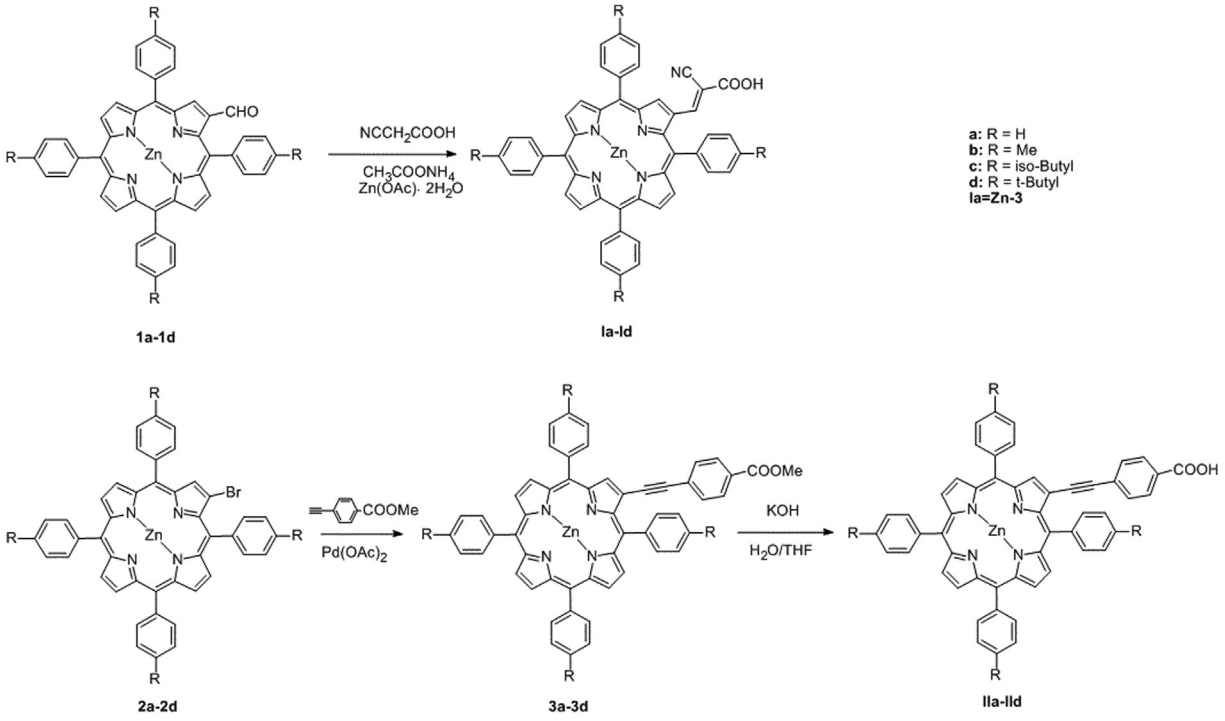

Scheme 1. Synthetic route of the porphyrin sensitizers **Ia**–**Id** and **IIa**–**IId**.

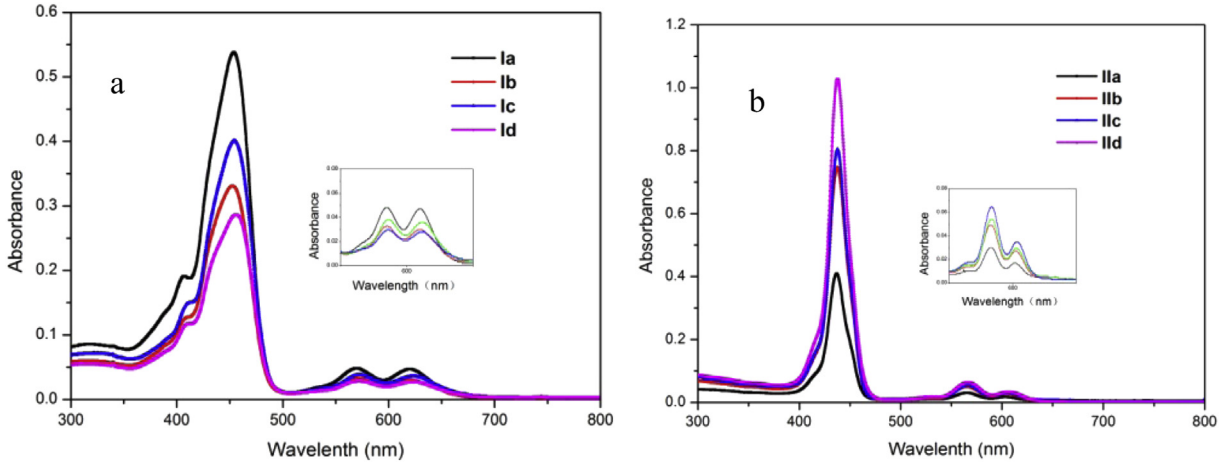

Fig. 2. UV–Vis absorption spectra of **Ia** ~ **Id** (a) and **IIa** ~ **IId** (b) in CH_2Cl_2 solution (3.0×10^{-6} M) and TiO_2 films (b).

some modification. Take **3a** as an example. The solution of compound **2a** (22.7 mg), $Pd(OAc)_2$ (4.6 mg), PPh_3 (3.1 mg), tetrabutylamine acetate (18 mg) and methyl 4-ethynylbenzoate (9.8 mg) in dry DMF (10 mL) was heated at 60 °C for 12 h under a nitrogen atmosphere. Then the solvent was washed by water (50 mL × 2). The resulting mixture was submitted to column chromatography using dichloromethane as eluent, collecting the major red fraction gives **3a** (13.2 mg, 37.4%) as purple powder. ^{1}H NMR (400 MHz, $CDCl_3$) δ 9.25 (s, 1H,$H_{\beta\text{-pyrrolic}}$), 8.92 (d, J = 7.3 Hz, 4H,$H_{\beta\text{-pyrrolic}}$), 8.88 (d, J = 4.7 Hz, 1H,$H_{\beta\text{-pyrrolic}}$), 8.77 (d, J = 4.7 Hz, 1H,$H_{\beta\text{-pyrrolic}}$), 8.29–8.17 (m, 8H, $H_{o\text{-Ph}}$), 7.95 (d, J = 8.2 Hz, 2H, $H_{2,6}$), 7.84–7.69 (m, 9H,$H_{m,p\text{-Ph}}$), 7.66 (t, J = 7.4 Hz, 2H, $H_{m\text{-Ph}}$), 7.60 (t, J = 7.3 Hz, 1H, $H_{p\text{-Ph}}$), 7.42 (d, J = 8.2 Hz, 2H, $H_{3,5}$), 3.91 (s, 3H,OCH_3). MS (MALDI-TOF) m/z found 834.3(M^+) (calcd. for $C_{54}H_{34}N_4O_2Zn^+$ 834.1973).

3b: 20.3 mg, yield 42.3%. ^{1}H NMR (400 MHz, $CDCl_3$) δ 9.28 (s,1H,$H_{\beta\text{-pyrrolic}}$), 8.96 (d, J = 8.8 Hz,4H,$H_{\beta\text{-pyrrolic}}$), 8.92 (d, J = 4.7 Hz, 1H,$H_{\beta\text{-pyrrolic}}$), 8.85 (d, J = 4.7 Hz, 1H,$H_{\beta\text{-pyrrolic}}$), 8.15–8.06 (m, 10H, $2H_{2,6}$+$H_{o\text{-Ph}}$), 7.60–7.55 (m,6H,$H_{m\text{-Ph}}$), 7.47–7.42 (m, 4H,$2H_{m\text{-Ph}}$+$2H_{3,5}$), 3.98 (s, 3H,OCH_3), 2.73 (s, 9H,CH_3), 2.45 (s, 3H,CH_3). MS (MALDI-TOF) m/z found 890.4(M^+) (calcd. for $C_{58}H_{42}N_4O_2Zn^+$ 890.2599).

3c: 15.7 mg, yield 40.3%. ^{1}H NMR (400 MHz, $CDCl_3$) δ 9.30 (s, 1H,$H_{\beta\text{-pyrrolic}}$), 8.95 (d, J = 2.3 Hz, 4H,$H_{\beta\text{-pyrrolic}}$), 8.91 (d, J = 4.7 Hz, 1H,$H_{\beta\text{-pyrrolic}}$), 8.79 (d, J = 4.7 Hz, 1H,$H_{\beta\text{-pyrrolic}}$), 8.18–8.08 (m, 8H,$H_{o\text{-Ph}}$), 8.02 (d, J = 8.2 Hz, 2H,$H_{2,6}$), 7.57–7.50 (m, 6H,$H_{m\text{-Ph}}$), 7.43 (d, 4H,$2H_{m\text{-Ph}}$+$2H_{3,5}$), 3.98 (s, 3H,OCH_3), 2.88–2.82 (m, 6H,–CH_2CH(CH_3)$_2$), 2.59 (d, J = 7.0 Hz, 2H,–CH_2CH(CH_3)$_2$), 2.24–2.14 (m, 3H,–CH_2CH(CH_3)$_2$), 2.08–2.01 (m, 1H,–CH_2CH(CH_3)$_2$), 1.21–1.13 (m, 18H,–CH_2CH(CH_3)$_2$), 1.06 (d, J = 6.6 Hz, 6H,–CH_2CH(CH_3)$_2$). MS (MALDI-TOF) m/z found 1058.7(M^+) (calcd. for $C_{70}H_{66}N_4O_2Zn^+$ 1058.4477).

3d: 10.4 mg, yield 33.2%. ^{1}H NMR (400 MHz, $CDCl_3$) δ 9.31 (s, 1H,$H_{\beta\text{-pyrrolic}}$), 8.97 (d, J = 3.4 Hz, 4H,$H_{\beta\text{-pyrrolic}}$), 8.91 (d, J = 4.7 Hz, 1H,$H_{\beta\text{-pyrrolic}}$), 8.74 (d, J = 4.8 Hz, 1H,$H_{\beta\text{-pyrrolic}}$), 8.20–8.11 (m, 8H, $H_{o\text{-Ph}}$), 7.99 (d, J = 8.2 Hz, 2H, $H_{2,6}$), 7.82–7.74 (m, 6H,$H_{m\text{-Ph}}$), 7.67 (d, J = 8.1 Hz, 2H,$H_{m\text{-Ph}}$), 7.44 (d, J = 8.3 Hz, 2H, $H_{3,5}$), 3.97 (s, 3H,OCH_3), 1.67–1.61 (m, 27H,CH_3), 1.36 (s, 9H,CH_3). MS (MALDI-TOF) m/z found 1058.7(M^+) (calcd. for $C_{70}H_{66}N_4O_2Zn^+$ 1058.4477).

Compounds **IIa**–**IId** were synthesized through a similar procedure. Take **IIa** as an example. A solution of KOH (10 mg) in H_2O (3.0 mL) was added into a solution of **3a** (12.3 mg) in THF (8.0 mL) and ethanol (2.0 mL), and was heated at reflux for 1 h. The solution was acidized by HCl and washed by H_2O (50mL × 2). The residue was purified by column chromatography using CH_2Cl_2/MeOH(100:1,v/v) as eluent, gave ***IIa*** (11,3 mg, 90%) as a dark-green solid. ^{1}H NMR (400 MHz, DMSO) δ 8.96 (s, 1H,$H_{\beta\text{-pyrroic}}$), 8.76 (d, J = 9.9 Hz, 4H,$H_{\beta\text{-pyrroic}}$), 8.71 (d, J = 4.7 Hz, 1H,$H_{\beta\text{-pyrroic}}$), 8.59 (d, J = 4.7 Hz, 1H,$H_{\beta\text{-pyrroic}}$), 8.24–8.10 (m, 8H,$H_{o\text{-Ph}}$), 7.87–7.68 (m, 14H,12$H_{m,p\text{-Ph}}$+$2H_{2,6}$), 7.22 (d, J = 8.0 Hz, 2H,$H_{3,5}$). MS (MALDI-TOF) m/z found 820.4(M^+) (calcd. for $C_{53}H_{32}N_4O_2Zn^+$ 820.1817). UV–vis (CH_2Cl_2) λ_{max} (log ε): 436.8(5.13), 565.8(4.00), 604.2(3.75) nm.

IIb: 13.6 mg, yield 94.3%. ^{1}H NMR (400 MHz, DMSO) δ 13.16 (s,br,1H,COOH) 9.01 (s, 1H,$H_{\beta\text{-pyrroic}}$), 8.79–8.71 (m, 5H,$H_{\beta\text{-pyrroic}}$),

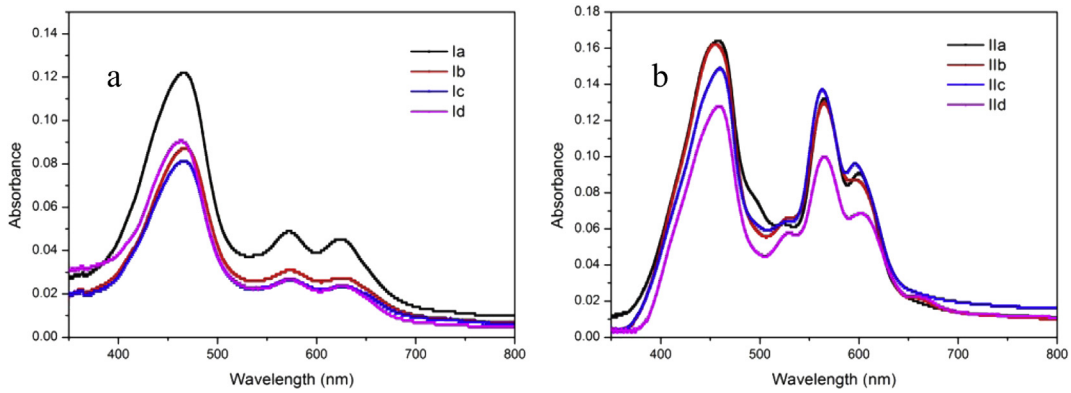

Fig. 3. UV–Vis absorption spectra of **Ia** ~ **Id** (a) and **IIa** ~ **IId** (b) on TiO_2 films.

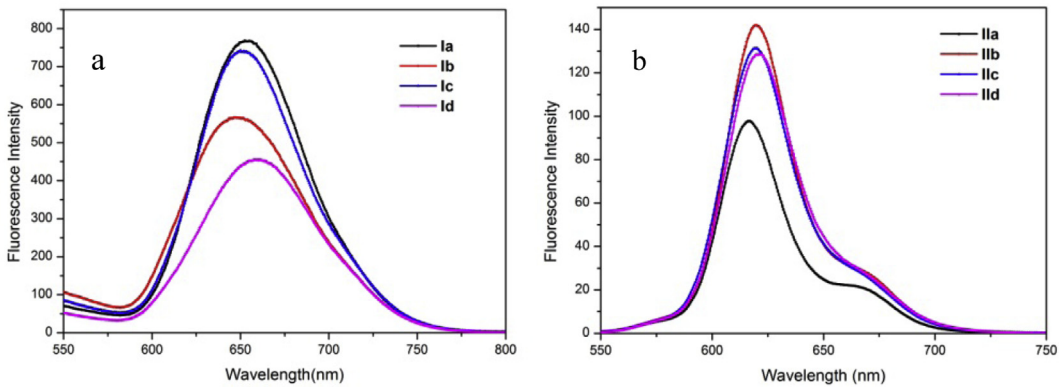

Fig. 4. Fluorescence spectrum of **Ia**–**Id** (a) and **IIa**–**IId** (b) in CH_2Cl_2 solution (3.0×10^{-6} M).

8.64 (d, J = 4.7 Hz, 1H,$H_{\beta\text{-pyrroic}}$), 8.13–7.91 (m, 10H, $8H_{o\text{-Ph}}$+$2H_{2,6}$), 7.66–7.55 (m, 6H,$H_{m\text{-Ph}}$), 7.49 (d, J = 7.9 Hz, 2H,$H_{m\text{-Ph}}$), 7.45 (d, J = 8.2 Hz, 2H, $H_{3,5}$), 2.70–2.64 (m, 9H,CH_3), 2.46 (s, 3H,CH_3). MS (MALDI-TOF) m/z found 876.4(M^+) (calcd. for $C_{57}H_{40}N_4O_2Zn^+$ 876.2433). UV–vis (CH_2Cl_2) λ_{max} (log ε): 438.0(5.40), 565.6(4.21), 604.8(3.95) nm.

IIc: 11.2 mg, yield 92.3%.^{1}H NMR (400 MHz, DMSO) δ 13.14 (s,br,1H,COOH), 9.01 (s, 1H,$H_{\beta\text{-pyrroic}}$), 8.75 (d, J = 6.5 Hz, 4H,$H_{\beta\text{-pyrroic}}$), 8.71 (d, J = 4.7 Hz, 1H,$H_{\beta\text{-pyrroic}}$), 8.57 (d, J = 4.6 Hz, 1H,$H_{\beta\text{-pyrroic}}$), 8.12–8.00 (m, 8H,$H_{o\text{-Ph}}$), 7.95 (d, J = 8.2 Hz, 2H,$H_{2,6}$), 7.60–7.53 (m, 6H,$H_{m\text{-Ph}}$), 7.47–7.41 (m, 4H2$H_{m\text{-Ph}}$+$2H_{3,5}$), 2.83–2.77 (m, 6H,–C**H**$_2$CH(CH_3)$_2$), 2.56 (d, J = 7.0 Hz, 2H,–C**H**$_2$CH(CH_3)$_2$), 2.13–2.18 (m,3H,–CH_2C**H**(CH_3)$_2$), 2.02–1.92 (m, 1H,–CH_2C**H**(CH_3)$_2$), 1.13–1.09 (m, 18H,–CH_2CH(C**H**$_3$)$_2$), 0.97 (d, J = 6.6 Hz, 6H,–CH_2CH(C**H**$_3$)$_2$). MS (MALDI-TOF) m/z found 1044.6(M^+) (calcd. for $C_{69}H_{64}N_4O_2Zn^+$ 1044.4321). UV–vis (CH_2Cl_2) λ_{max} (log ε): 438.0(5.43), 567.2(4.26), 606.0(4.00) nm.

IId: 9.1 mg, yield 90.2%. ^{1}H NMR (400 MHz, DMSO) δ 13.14 (s,br,1H,COOH),8.98 (s, 1H,$H_{\beta\text{-pyrroic}}$), 8.83–8.72 (m, 4H,$H_{\beta\text{-pyrroic}}$), 8.70 (d, J = 4.7 Hz, 1H,$H_{\beta\text{-pyrroic}}$), 8.54 (d, J = 4.6 Hz, 1H,$H_{\beta\text{-pyrroic}}$), 8.16–8.01 (m, 8H,$H_{o\text{-Ph}}$), 7.91 (d, J = 8.2 Hz, 2H,$H_{2,6}$), 7.81–7.74 (m, 6H,$H_{m\text{-Ph}}$), 7.66 (d, J = 8.0 Hz, 2H,$H_{m\text{-Ph}}$), 7.44 (d, J = 8.2 Hz, 2H,$H_{3,5}$), 1.66–1.60 (m, 27H,CH_3), 1.28 (s, 9H,CH_3). MS (MALDI-TOF) m/z found 1044.7(M^+) (calcd. for $C_{69}H_{64}N_4O_2Zn^+$ 1044.4321). UV–vis (CH_2Cl_2) λ_{max} (log ε): 437.8(5.53), 567.2(4.34), 606.2(4.07) nm.

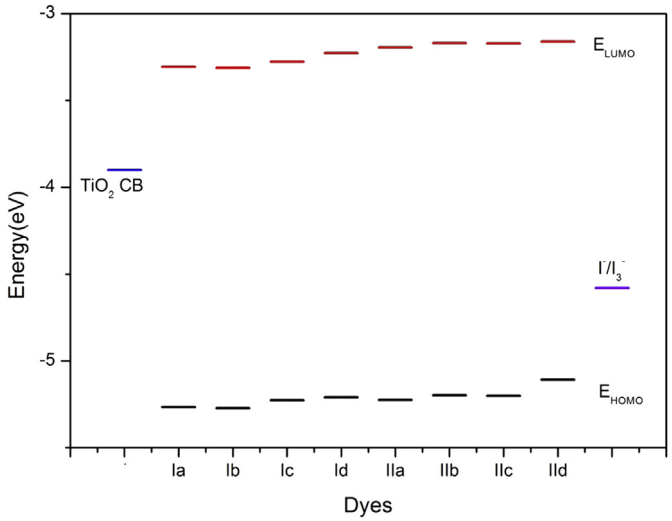

Fig. 5. Energy level diagram of dyes **Ia**–**Id** and **IIa**–**IId**, the electrolyte and TiO_2.

3. Results and discussion

3.1. Synthesis

The synthetic routes of sensitizers **Ia**–**Id** were depicted in Scheme 1. Compounds **1a**–**1d** were employed as the starting materials. Followed by Knoevenagel condensation with cyanoacetic acid in a solution of CH_3COOH/THF(1:1,v/v), in which zinc acetate and ammonium acetate functional as catalysts, to give products **Ia**–**Id**. Dye **Ia**, which being known as **Zn-3** reported by Gratzel [25], was used as a reference dye in this study.

The synthetic route of sensitizers **IIa**–**IId** was depicted in Scheme 1, too. Compounds **2a**–**2d** [26] were employed as the starting materials and treated with 4-ethynyl methyl benzoate to undergo Sonogashira coupling to give **3a**–**3d**. The target molecular **IIa**–**IId** were given by subsequent treatment with base in a mixture of THF and water. The molecular structures were verified by ^{1}H NMR and MALDI-TOF mass spectrometry.

3.2. Photophysical properties

The UV–visible adsorption spectra of zincporphyrins used for the photovoltaic measurements were measured in CH_2Cl_2. The adsorption maxima and absorption coefficients of these porphyrins are listed in Table 1. The UV–visible absorption spectrum of **Ia** ~ **Id** and **IIa** ~ **IId** are shown in Fig. 2, these molecular exhibit characteristic porphyrin spectra [28]: strong Soret band is near 430 nm (**Ia**–**Id** are near 450 nm) and weaker Q bands are in the region of 550–650 nm. The typical strong Soret band and moderate band are assigned to the π–π^* transitions of the conjugated system, arising from the porphyrin skeleton.

Table 2
Electrochemical properties of series dyes.

Dye	Eox[a] V (vs. Fc/Fc+)	E_{0-0}[b] eV	E_{HOMO}[c] eV	E_{LUMO}[d] eV
Ia	0.466	1.96	−5.266	−3.306
Ib	0.472	1.96	−5.272	−3.312
Ic	0.426	1.95	−5.226	−3.276
Id	0.410	1.94	−5.210	−3.226
IIa	0.425	2.03	−5.225	−3.195
IIb	0.399	2.03	−5.199	−3.169
IIc	0.401	2.03	−5.201	−3.171
IId	0.380	2.02	−5.180	−3.160

[a] First oxidation potentials(vs. Fc/Fc+).
[b] Determined from the intercept of the normalized absorption and emission spectra.
[c] $E_{HOMO} = -[4.8 + Eox$ (vs. Fc/Fc+)] eV.
[d] $E_{LUMO} = [E_{HOMO} + E_{0-0}]$ eV.

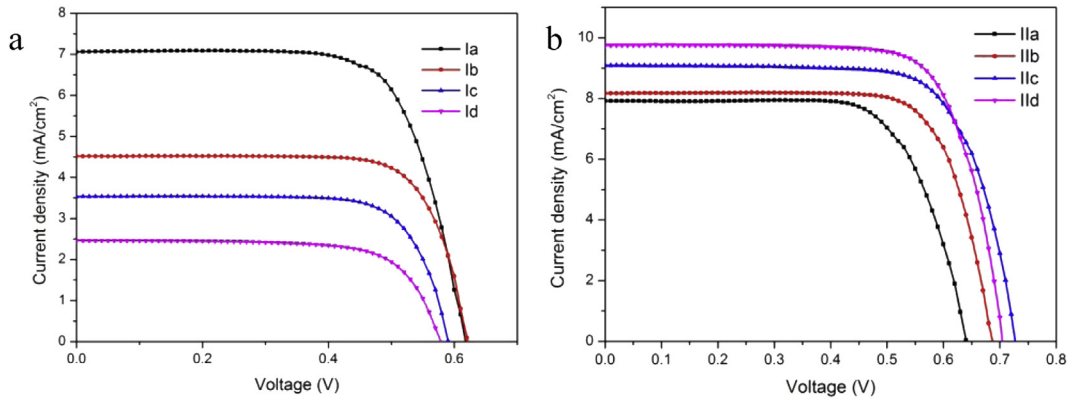

Fig. 6. Current density–voltage characteristics for DSSCs based on the porphyrin dyes **Ia**–**Id** (a) and **IIa**–**IId** (b).

The Fluorescence spectrum of the porphyrins was measured in CH_2Cl_2. The emission maxima were summarized in Table 1. The fluorescence spectrum of **Ia**–**Id** and **IIa**–**IId** were shown in Fig. 4. The shape and peak positions of the spectra are analogous for the compounds which having same linker implying the electronic structure of the porphyrin core is not disturbed largely by the substituents on *meso*-position [19].

Fig. 3 shows the absorption spectra of **Ia** ~ **Id** and **IIa** ~ **IId** adsorbed on TiO_2 films. As seen from Fig. 3, the absorption spectra of dyes adsorbed on TiO_2 films are similar to those corresponding solution spectra, but obviously red-shifted and broadened due to the formation of the J-type aggregates of porphyrins on the TiO_2 surface [21,29].

3.3. Electrochemical properties

To evaluate the electron injection from the excited state of the dyes to the CB of TiO_2 electrode, the electrochemical behaviors of the dyes were studied by cyclic voltammetry (CV), Fig. 5 compares the HOMO/LUMO potentials of **Ia** ~ **Id** and **IIa** ~ **IId** with those of the electrolyte and the conduction band of TiO2, This diagram is based on the literature reports and the experimental results. The CV curves of **Ia** ~ **Id** and **IIa** ~ **IId** are depicted in Figs. S1 and S2 in Supporting Information, and the data are summarized in Table 2. All porphyrin sensitizers exhibit reversible waves for the first oxidation, corresponding to the HOMO energy of the dye. For instance, the first oxidation potentials (*E*ox) (vs. Fc/Fc^+) of **Ia** and **IId** were determined to be 0.466 and 0.380 V, respectively. The HOMO values versus vacuum were transformed via the equation $E_{HOMO} = -[4.8 + E\text{ox (vs. Fc/Fc}^+)]$eV [30], and the corresponding E_{HOMO} of **Ia** and **IId** versus vacuum were −5.266 and −5.180 eV, respectively. The E_{LUMO} calculated by $[E_{HOMO} + E_{0-0}]$ were −3.306 and −3.158 eV, respectively, which the E_{0-0} were calculated from intersection of the normalized absorption and the emission spectra (λ_{int}) and $E_{0-0} = 1240/\lambda_{int}$. The results show that the HOMO levels of all the dyes are sufficiently higher than the energy level of I^-/I_3^- redox (−4.58 eV) [31]. It indicates the reason of oxidized formed which could accept electron from I^- ions and then be regenerated after electron having been injected into the CB of TiO_2. The LUMO levels of these dyes are significantly lower than the conduction band edge energy level of the TiO_2 electrode (−3.9 eV) [32], which providing an energy gap necessary for efficient electron injection. Hence, an effective electron transfer from the excited dye to TiO_2 could be occurred.

3.4. Photovoltaic performance of DSSCs

The photocurrent–voltage (*J*–*V*) curves of **Ia**–**Id** and **IIa**–**IId** and corresponding IPCE action spectra are depicted in Figs. 6 and 7, respectively. The detail parameters of photovoltaic performance, short-circuit current density (J_{sc}), open-circuit voltage (V_{oc}), fill factor (FF), and photovoltaic conversion efficiency (η), are summarized in Table 3. Since the TiO_2 films were not optimized in our lab to give an absolute η value for our sensitizers, the cell performances made from these sensitizers were compared with that from the known **Zn-3**(**Ia**) [25] under the same condition. It was found that under the same conditions, **Ia** sensitized cell is $\eta = 3.12\%$ with $J_{sc} = 7.06$ mA cm^{-2}, $V_{oc} = 0.62$ V, and FF = 0.71. **IId** sensitized cell shows $\eta = 5.08\%$ with $J_{sc} = 9.75$ mA cm^{-2}, $V_{oc} = 0.71$ V, and FF = 0.73, is the highest

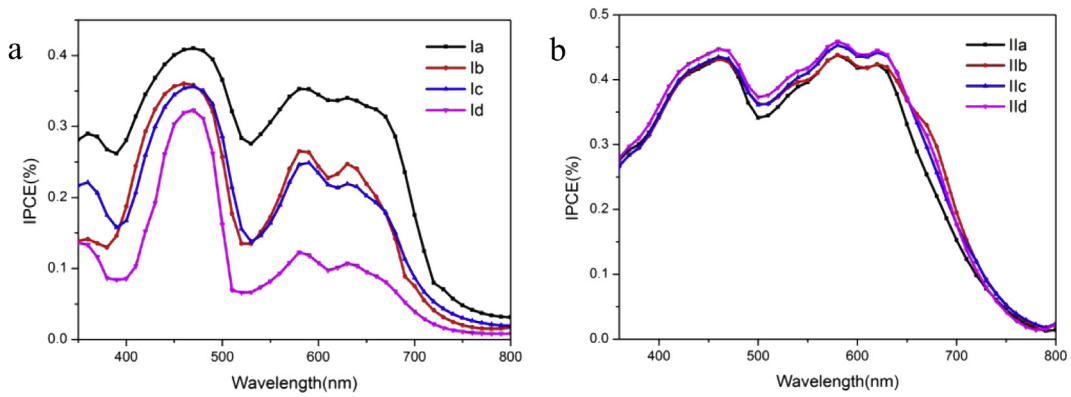

Fig. 7. IPCE spectra for DSSCs based on **Ia**–**Id** (a) and **IIa**–**IId** (b).

Table 3
Photovoltaic performance and the Γ value of DSSCs based on the porphyrin dyes.

Dye	J_{sc} (mA/cm^2)	V_{oc} (V)	FF (%)	η (%)	Γ (mol cm^{-2})
Ia	7.06	0.62	71.27	3.12	6.40×10^{-8}
Ib	4.52	0.63	74.44	2.12	2.61×10^{-8}
Ic	3.54	0.60	73.35	1.56	1.32×10^{-8}
Id	2.46	0.59	69.86	1.01	–
IIa	7.92	0.62	72.36	3.55	2.75×10^{-7}
IIb	8.17	0.69	74.18	4.18	2.01×10^{-7}
IIc	9.09	0.73	72.16	4.79	1.39×10^{-7}
IId	9.75	0.71	73.44	5.08	1.15×10^{-7}

Light source: 100 mW/cm^2, AM 1.5G simulated solar light; working area: 0.159 cm^2; thickness: 15 μm; Dye bath: EtOH solution (0.3 mM); Electrolyte: 0.06 M LiI, 0.03 M I_2, 0.6 M 1,2-dimethyl-3-propylimidazolium iodide (DMPII), and 0.5 M 4-tert-butylpyridine (TBP) in acetonitrile solution.

efficiency achieved in this study. **Id** sensitized cell exhibits $\eta = 1.01\%$ with $J_{sc} = 2.46$ mA cm^{-2}, $V_{oc} = 0.59$ V, and FF = 0.69, is the lowest efficiency achieved in this study. With different linkers on β position, substituents on *meso*-position have different influences on cell performance. For ethylene, cell performance decreased greatly as the size of *meso*-substituents increasing, but for phenyl ethynyl, cell performance increased with the size of *meso*-substituent increasing. Typical EIS Nyquist plots for DSSCs based on the **IIa**–**IId** are shown in Fig. 8. The larger semi-circle at lower frequency represents the interfacial charge transfer resistances (R_{ct}) at the TiO_2/dye/electrolyte interface, which can be deduced by fitting curves from the range of intermediated frequency using Z-view software. The fitted R_{ct} increases in the order of **Ia**(271.5Ω) < **Ib**(313.7Ω) < **Id**(377.5Ω) < **Ic**(409.7Ω), the same order as the V_{oc} values of these dyes **Ia**(620 mV) < **Ib**(690 mV) < **Id**(710 mV) < **Ic**(730 mV).

To investigate the relationship between *meso*-substituent and cell performance, we tested Γ value of all porphyrin sensitizers uptake on TiO_2 surface, the Γ value of **Id** was too low to be tested, and all data are also summarized in Table 3. We found that the Γ value of porphytin dyes with ethylene on β position dropped sharply with the size of *meso*-substituents increasing. It could be caused by the steric hindrance of *meso*-substituent, the dye adopting relatively parallel orientation to the TiO_2 surface and yielding to small surface coverage and low cell performance [33]. And with phenyl ethynyl, a much longer linker was compared with ethylene, the Γ value drops with the size of *meso*-substituent increasing, but the cell performance of these devices improved. It could be caused by the *meso*-substituents function as protect group which decrease the possibility of I_3^- penetrating the adsorbed dye layer, thus reducing the interfacial charge recombination [34]. Therefore, J_{SC} of **IIa**–**IId** -sensitized DSSCs increased with the size of *meso*-substituent increasing, and **IId** gives the best cell performance. Same *meso*-substituents give an opposite influence for different linker with different mechanics. This fact indicates the matching degree of linker length and the size of *meso*-substituent could be a key point to porphyrin structure that affecting the cell performance of the device based on porphyrin sensitizers.

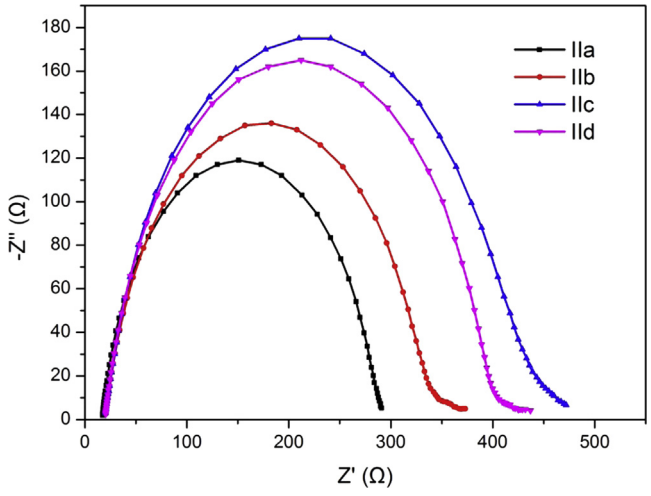

Fig. 8. EIS for DSSCs based on the **IIa**–**IId** dyes measured in the dark under −0.70 V displayed in the form of Nyquist plots.

4. Conclusions

In summary, we successfully synthesized 8 porphyrin sensitizers, and 6 of them were synthesized for the first time. Dyes with the same linker on β position have shown almost the same optical, electrochemical properties, indicating that different *meso*-substituents have little effect on these aspects. Various optical properties have been achieved by changing the linkers on β position. The cyclic voltammetry results of these 8 dyes suggest that the HOMO and LUMO levels of the dyes meet the requirement for their applications in DSSCs. The *meso*-substituents could affect the cell performance greatly. Different *meso*-substituents could affect the cell performance in both positive and negative ways by changing the linker, the matching degree of the length of linker and the size of *meso*-substituents could be a key point in porphyrin structures that affect the cell performance of the device based on porphyrin sensitizers.

Acknowledgment

This work is supported by National Natural Science Foundation of China (No. 21076147), Natural Science Foundation of Tianjin (No. 10JCZDJC23700), dependent Innovation Foundation of Tianjin University (2010) and International S&T Cooperation Program of China (No 2012DFG41980).

Appendix A. Supplementary material

Supplementary material related to this article can be found at http://dx.doi.org/10.1016/j.dyepig.2013.07.037.

References

[1] O'Regan B, Grätzel M. A low-cost, high-efficiency solar cell based on dye-sensitized colloidal TiO_2 films. Nature 1991;353:737–40.
[2] Campbell WM, Burrell AK, Officer DL, Jolley K. Porphyrins as light harvesters in the dye-sensitised TiO_2 solar cell. Coordin Chem Rev 2004;248:1363–79.
[3] Grätzel M. Solar energy conversion by dye-sensitized photovoltaic cells. Inorg Chem 2005;44:6841–51.
[4] Lee CW, Lu HP, Lan CM, Huang YL, Liang YR, Yen WN, et al. Novel zinc porphyrin sensitizers for dye-sensitized solar cells: synthesis and spectral, electrochemical, and photovoltaic properties. Chem Eur J 2009;15:1403–12.
[5] Nazeeruddin MK, Angelis FD, Fantacci S, Selloni A, Viscardi G, Liska P, et al. Combined experimental and DFT-TDDFT computational study of photoelectrochemical cell ruthenium sensitizers. J Am Chem Soc 2005;127:16835–47.
[6] Eu S, Hayashi S, Umeyama T, Oguro A, Kawasaki M, Kadota N, et al. Effects of 5-membered heteroaromatic spacers on structures of porphyrin films and photovoltaic properties of porphyrin-sensitized TiO2 cells. J Phys Chem C 2007;111:3528–37.
[7] Imahori H, Matsubara Y, Iijima H, Umeyama T, Matano Y, Ito S, et al. Effects of *meso*- diarylamino group of porphyrins as sensitizers in Dye-Sensitized Solar Cells on optical, electrochemical, and photovoltaic properties. J Phys Chem C 2010;114:10656–65.
[8] Na X, Xianwei H, Xiaoming F, Yijiang L, Bin Z, Lijun D, et al. The structural modification of thiophene-linked porphyrin sensitizers for dye-sensitized solar cells. Dyes Pigments 2011;88:75–83.
[9] Bessho T, Zakeeruddin SM, Yeh C, Diau EW, Grätzel M. Highly efficient mesoscopic Dye-Sensitized Solar Cells based on donor–acceptor-substituted porphyrins. Angew Chem Int Ed 2010;49:6646–9.

[10] Yella A, Lee HW, Tsao HN, Yi C, Chandiran AK, Nazeeruddin MK, et al. Porphyrin-sensitized solar cells with cobalt (II/III)–based redox electrolyte exceed 12 percent efficiency. Science 2011;334:629–33.
[11] Wang ZS, Cui Y, Hara K, Dan-oh Y, Kasada C, Shinpo A. A high-lightharvesting-efficiency coumarin dye for stable dye-sensitized solar cells. Adv Mater 2007;19:1138–41.
[12] Seo KD, Song HM, Lee MJ, Pastore M, Anselmi C, Angelis FD, et al. Coumarin dyes containing low-band-gap chromophores for dye-sensitised solar cells. Dyes Pigments 2011;90:304–10.
[13] Hara K, Wang ZS, Sato T, Furube A, Katoh R, Sugihara H, et al. Oligothiophene-necontaining coumarin dyes for efficient dye-sensitized solar cells. J Phys Chem B 2005;109:15476–82.
[14] Edvinsson T, Li C, Pschirer N, Schöneboom J, Eickmeyer F, Sens R, et al. Intramolecular charge-transfer tuning of perylenes: spectroscopic features and performance in dye-sensitized solar cells. J Phys Chem C 2007;111:15137–40.
[15] Eu S, Katoh T, Umeyama T, Matano Y, Imahori H. Synthesis of sterically hindered phthalocyanines and their applications to dye-sensitized solar cells. Dalton Trans 2008:5476–83.
[16] Xu W, Peng B, Chen J, Liang M, Cai F. New phenylamine-based dyes for dye-sensitized solar cells. J Phys Chem 2008;112:874–80.
[17] Zhang XH, Wang ZS, Cui Y, Koumura N, Furube A, Hara K. Organic sensitizers based on hexylthiophene-functionalized Indolo[3,2-b]carbazole for efficient dye-sensitized solar cells. J Phys Chem C 2009;113:13409–15.
[18] Lin CY, Lo CF, Lu HP, Hung CS, Diau WG. Design and characterization of novel porphyrins with oligo(phenylethylnyl) links of varied length for dye-sensitized solar cells: synthesis and optical, electrochemical, and photovoltaic investigation. J Phys Chem C 2009;113(2):755–64.
[19] Mao JY, He NN, Ning ZJ, Zhang Q, Guo FL, Tian H, et al. Stable dyes containing double acceptors without COOH as anchors for highly efficient Dye-Sensitized Solar Cells. Angew Chem Int Ed 2012;51:9873–6.
[20] Imahori H, Hayashi S, Hayashi H, Oguro A, Eu S, Umeyama T, et al. Effects of porphyrin substituents and adsorption conditions on photovoltaic properties of porphyrin-sensitized TiO_2 cells. J Phys Chem C 2009;113(42):18406–13.
[21] Chang YC, Wang CL, Pan TY, Hong SH, Lan CM, Kuo HH, et al. A strategy to design highly efficient porphyrin sensitizers for dye- sensitized solar cells. Chem Commun 2011;47:8910–2.
[22] Li G, Jiang K, Bao P, Li Y, Li S, Yang L. Molecular design of triarylamine-based organic dyes for efficient dye-sensitized solar cells. New J Chem 2009;33:868–76.
[23] Yanagida M, Yamaguchi T, Kurashige M, Fujihashi G, Hara K, Katoh R, et al. Nanocrystalline solar cells sensitized with monocarboxyl or dicarboxyl pyridylquinoline Ruthenium(II) complexes. Inorg Chim Acta 2003;351:283–90.
[24] Ito S, Chen P, Comte P, Nazeeruddin MK, Liska P, Péchy P, et al. Fabrication of screen-printing pastes from TiO_2 powders for Dye-Sensitised Solar Cells. Prog Photovoltaics Res Appl 2007;15:603–12.
[25] Campbell WM, Jolley KW, Wagner P, Wagner K, Walsh PJ, Gordon KC, et al. Highly efficient porphyrin sensitizers for dye-sensitized solar cells. J Phys Chem C 2007;111:11760–2.
[26] Wang Q, Campbell WM, Bonfantani EE, Jolley KW, Officer DL, Walsh PJ, et al. Efficient light harvesting by using green Zn-porphyrin-sensitized nanocrystalline TiO_2 films. J Phys Chem B 2005;109:15397–409.
[27] Gao GY, Ruppel JV, Allen DB, Chen Y, Zhang XP. Synthesis of *â*-functionalized porphyrins via palladium-catalyzed carbon-heteroatom bond formations: expedient entry into *â*-chiral porphyrins. J Org Chem 2007;72:9060–6.
[28] Gouterman MJ. Spectra of porphyrins. J Mol Spectrosc 1961;6:138–63.
[29] Lo CF, Luo L, Diau WG, Chang IJ, Lin CY. Evidence for the assembly of carboxyphenylethynyl zinc porphyrins on nanocrystalline TiO_2 surfaces. Chem Commun 2006:1430–2.
[30] Jones BA, Facchetti A, Wasielewski MR, Marks TJ. Tuning orbital energetics in arylene diimide semiconductors. Materials design for ambient stability of n-type charge transport. J Am Chem Soc 2007;129:15259–78.
[31] Lenzmann F, Krueger J, Burnside S, Brooks K, Grätzel M, Gal D, et al. Surface photovoltage spectroscopy of Dye-Sensitized Solar Cells with TiO_2, Nb_2O_5, and $SrTiO_3$ nanocrystalline photoanodes: indication for electron injection from higher excited dye states. J Phys Chem B 2001;105:6347–52.
[32] Cao XW, Lin WY, Yu QX. A ratiometric fluorescent probe for thiols based on a Tetrakis (4-hydroxyphenyl)porphyrin coumarin Scaffold. J Org Chem 2011;76:7423–30.
[33] Mathew S, Iijima H, Toude Y, Umeyama T, Matano Y, Ito S, et al. Optical, electrochemical and photovoltaic effects of an electron-withdrawing tetrafluorophenylene bridge in a push pull porphyrin sensitizer used for Dye-Sensitized Solar Cells. J Phys Chem C 2011;115(29):14415–24.
[34] Xu YJ, Liang M, Liu XJ, Han HY, Sun Z, Xue S. Synthesis of triarylamine dyes containing secondary electron-donating groups and application in the dye-sensitized solar cells. Synth Metal 2011;161(5–6):496–503.